# Control of Energy Density inside a Disordered Medium by Coupling to Open or Closed Channels

Raktim Sarma,[1] Alexey G. Yamilov,[2,*] Sasha Petrenko,[2] Yaron Bromberg,[1] and Hui Cao[1,†]
[1]Department of Applied Physics, Yale University, New Haven, Connecticut 06520, USA
[2]Department of Physics, Missouri University of Science & Technology, Rolla, Missouri 65409, USA
(Received 6 June 2016; published 17 August 2016)

We demonstrate experimentally the efficient control of light intensity distribution inside a random scattering system. The adaptive wave front shaping technique is applied to a silicon waveguide containing scattering nanostructures, and the on-chip coupling scheme enables access to all input spatial modes. By selectively coupling the incident light to the open or closed channels of the disordered system, we not only vary the total energy stored inside the system by a factor of 7.4, but also change the energy density distribution from an exponential decay to a linear decay and to a profile peaked near the center. This work provides an on-chip platform for controlling light-matter interactions in turbid media.

DOI: 10.1103/PhysRevLett.117.086803

It has long been known that in disordered media there are many fascinating and surprising effects resulting from the interferences of multiply scattered waves [1,2]. One of them is the creation of transmission eigenchannels, which can be broadly classified as either open or closed [3,4]. The existence of high-transmission (open) channels allows for an optimally prepared coherent input beam to be transmitted through a lossless diffusive medium with order unity efficiency. In contrast, waves injected into low-transmission (closed) channels barely penetrate the medium and are mostly reflected. In general, the penetration depth and energy density distribution of multiply scattered waves inside a disordered medium are determined by the spatial profiles of the transmission eigenchannels that are excited by the incident light. The distinct spatial profiles of the open and closed channels suggest that selective coupling of incident light to these channels enables the effective control of the total transmission and energy distribution inside the random medium [5,6]. Since the energy density determines the light-matter interactions inside a scattering system, manipulating its spatial distribution opens the door to tailoring optical excitations as well as linear and nonlinear optical processes such as absorption, emission, amplification, and frequency mixing inside turbid media. The potential applications range from photovoltaics [7,8], white light emitting diodes [9], and random lasers [10], to biomedical sensing [11] and radiation treatments [12].

In recent years there have been numerous theoretical and experimental studies on transmission eigenchannels [5,13–17]. While by knowing the transmission matrix one can determine their profiles [18–21], it is difficult to directly probe their spatial profiles inside three-dimensional (3D) random media. So far, open and closed channels have been observed only with an acoustic wave inside a two-dimensional (2D) disordered waveguide [22], but controlling the energy density distribution has not been realized due to the lack of an efficient wave front modulator for acoustic wave or microwave radiation. The advantage of optical waves is the availability of spatial light modulators (SLMs) with many degrees of freedom. However, the commonly used samples in an optical experiment have an open slab geometry, thus making it impossible to control all input modes due to the limited numerical aperture of the imaging optics. Such incomplete control dramatically weakens the open channels [23], although a notable enhancement of the total transmission has been achieved [20,24]. Furthermore, an enhancement of the total energy stored inside a 3D scattering sample has been reported [25], but a direct probe and control of the optical intensity distribution inside the scattering medium are still missing.

In this Letter, we demonstrate experimentally the control of the energy density distribution inside a scattering medium. Instead of the open slab geometry, we fabricate a silicon waveguide that contains scatterers and has reflecting sidewalls. The intensity distribution inside the two-dimensional waveguide is probed from the third dimension. With careful design of the on-chip coupling waveguide, we can access all the input modes. Such control of the incident wave front enables an order of magnitude enhancement of the total transmission or a 50 times suppression. A direct probe of the optical intensity distribution inside the disordered waveguide reveals that the selective excitation of the open channels results in the buildup of energy deep inside the scattering medium, while the excitation of the closed channels greatly reduces the penetration depth. Compared to the linear decay for random input fields, the optimized wave front can produce an intensity profile that either is peaked near the center of the waveguide or decays exponentially with depth. The total energy stored inside the waveguide is increased 3.7 times or decreased 2 times.

The 2D waveguide structure was fabricated in a 220 nm silicon layer on top of a 3 $\mu$m buried oxide by electron beam lithography and reactive ion etching [6]. As shown in Fig. 1, air holes are randomly distributed within the waveguide whose sidewalls are a photonic crystal that reflects light. At the probe wavelength $\lambda = 1.51\ \mu$m, the transport mean free path $\ell = 2.5\ \mu$m is much less than the length $L = 50\ \mu$m of the disordered waveguide, so that the light transport is diffusive. The out-of-plane scattering, which provides a direct probe of the light transport inside the random structure, can be treated as loss and the diffusive dissipation length is $\xi_a = 31\ \mu$m. The values of $\ell$ and $\xi_a$ were extracted from the measured intensity distribution and intensity fluctuations inside the disordered waveguide for uncontrolled illumination [26]. The waveguide of width $W = 15\ \mu$m supports $N = 56$ transmission eigenchannels, among which ~5 are open channels and the rest are closed channels. The total transmission for the uncontrolled illumination is about 4.8%.

The probe light is injected into the waveguide from the edge of the wafer. Because of the large mismatch of the refractive index between silicon and air, the light can be coupled only to the lower-order modes of the ridge waveguide. This limits the number of input modes that can be controlled by wave front shaping. To increase the degree of input control, the coupling waveguide (lead) is tapered at an angle of 15° [Fig. 1(a)]. The wider waveguide at the front end supports many more lower-order modes, which can be excited by the incident light and then converted to high-order modes by the taper [27]. As detailed in the Supplemental Material [27], we set $W_1 = 330\ \mu$m for the fabricated sample in Fig. 1, so that the number of waveguide modes excited at the air-silicon interface is significantly larger than $N$. This ensures all input modes to the disordered waveguide are accessed by the incident fields with phase-only modulation.

The wave front shaping experiment is shown schematically in Fig. 2(a) and detailed in the Supplemental Material [27]. A monochromatic laser beam is phase modulated by a SLM and then focused to the edge of the wafer by a microscope objective of numerical aperture (NA) 0.7. To produce a line of illumination at the input facet of the coupling waveguide, the SLM imposes phase modulation only along one dimension that is parallel to the transverse direction of the waveguide, as shown by the 2D phase mask in Fig. 2(a). The light that is scattered out of plane by the random array of air holes is collected by an objective and projected to an InGaAs camera to obtain the spatial

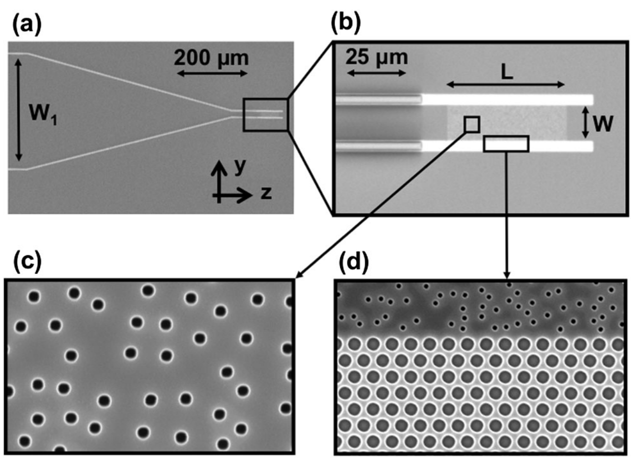


FIG. 1. On-chip disordered waveguide with a tapered lead. (a) Top-view scanning electron micrograph (SEM) of a fabricated silicon waveguide. A ridge waveguide (lead) is tapered from the width $W_1 = 330\ \mu$m at the edge of the wafer to the width $W = 15\ \mu$m, in order to increase the degree of control of the light that is injected to the disordered waveguide. (b) Magnified SEM of the disordered region of the waveguide that consists of a random array of air holes (diameter = 90 nm). (c) Magnified SEM showing the air holes distributed randomly within the waveguide with a filling fraction of 6%. (d) The sidewalls of the waveguide are made of a triangular lattice of air holes (diameter = 360 nm) with a lattice constant of 505 nm, which supports a full photonic band gap at the wavelength $\lambda = 1.51\ \mu$m.

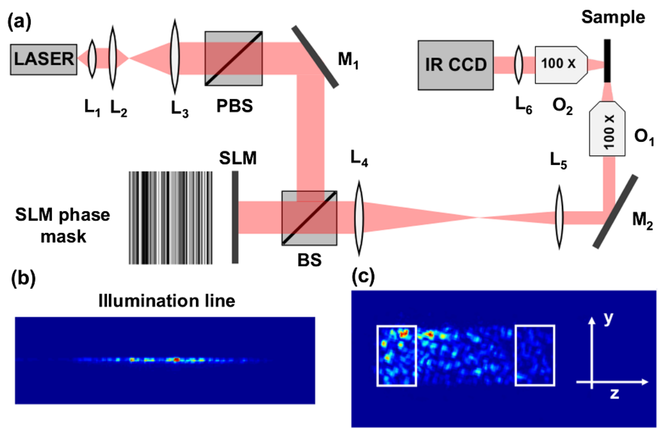


FIG. 2. Wave front shaping experiment to control the intensity distribution inside a disordered waveguide. (a) A schematic of the experimental setup. Laser (HP 8168F) output at $\lambda = 1510$ nm is collimated (by lens $L_1$), expanded (by $L_2$, $L_3$), and linearly polarized (by a polarized beam splitter PBS) before being modulated by a phase-only SLM (Hamamatsu X10468). Two lenses ($L_4$, $L_5$) are used to project the SLM plane to the pupil plane of an objective $O_1$ (100×, NA = 0.7), and the edge of the wafer is placed at the focal plane. The SLM imposes phase modulation only in one direction in order to generate a line at the front end of the coupling waveguide. A sample phase pattern on the SLM is shown. The light scattered out of the sample plane is collected by another objective $O_2$ (100×, NA = 0.7) and imaged to an InGaAs camera (Xenics XEVA 1.7-320) by a tube lens ($L_6$). $M_1$ and $M_2$ are mirrors and BS is a beam splitter. (b) An optical image of the illumination line ($330 \times 1.1\ \mu$m) on the waveguide facet. The input intensity is modulated along the line. (c) An image of the spatial distribution of the light intensity inside the disordered waveguide for a random input wave front. The spatial resolution is about 1.1 $\mu$m. The ratio $S$ of the integrated intensities over the two rectangles at the back and front side of the waveguide is used as feedback for optimizing the input wave front.

distribution of the intensity $I(y,z)$ inside the disordered structure [Fig. 2(c)].

Two wave front shaping approaches have been developed for the transmission enhancement: one is based on the measurement of the transmission matrix [28,29]; the other relies on feedback [30]. While the open channels can be obtained from the measured transmission matrix, the closed channels are subject to measurement noise due to the nearly vanishing transmission. Here, we took the feedback approach, and optimized the procedure using the continuous sequential algorithm [30] to control the energy density inside the disordered waveguide. The cost function $S$ is the ratio of the light intensity integrated over an area in the back part of the waveguide to that in the front part [marked by two rectangles in Fig. 2(c)].

First, we maximize $S$ to enhance the light penetration into the scattering structure. Figure 3(b) shows the final intensity distribution $I(y,z)$ for the optimized input. In Fig. 3(e) we plot the cross-section-averaged intensity $I(z) = \int_0^W I(y,z)dy$, further averaged over four wavelengths and three initial phase patterns that served as the seed to the optimization algorithm [27]. $I(z)$ is peaked near the center of the disordered waveguide in Fig. 3(e), which is dramatically different from the monotonic decay with random input fields in Fig. 3(d). The latter profile is in agreement with the prediction of diffusion theory and the slight deviation from a linear decay is caused by the out-of-plane scattering loss. The dissipation causes an asymmetry in the optimized intensity distribution with respect to the center of the waveguide ($z/L = 0.5$), as the peak of $I(z)$ in Fig. 3(b) shifts towards the input end. Such an asymmetry is captured by the maximum transmission channel, but not by the fundamental diffusion mode [25] or the return probability [5]. The resemblance of the optimized $I(z)$ to the spatial profile of the open channels indicates that the optimized wave front couples light to the high-transmission eigenchannels.

Next, we minimize $S$ by adapting the input wave front, and the resulting intensity distribution is presented in Fig. 3(c). The cross-section-averaged intensity $I(z)$ in Fig. 3(f) exhibits a much faster decay with depth than the random input. Moreover, the decay is clearly exponential, resembling the spatial profile of the closed channels. Despite the presence of measurement noise, the optimized wave front couples effectively to the low-transmission eigenchannels.

To confirm the experimental results, we simulate a 2D disordered waveguide with all parameters equal to the experimental values [27,31]. The phase-only modulation is imposed on the input wave front to optimize the same cost function $S$ with the continuous sequential algorithm (details in the Supplemental Material) [27]. The solid curves in Figs. 3(d)–3(f) represent the simulation results, which agree well with the experimental data. The curves are normalized such that the total incoming flux is equal to unity in all cases. Therefore, the intensity profiles can be quantitatively compared to get the order of magnitude of the intensity amplification within the scattering sample.

By projecting the optimized fields onto the transmission eigenchannels, we obtain the contributions from the individual channels. Figure 4(a) presents the weight $w$ of each channel as a function of the transmission eigenvalue $\tau$ in the case that the cost function $S$ is maximized [Figs. 3(b) and 3(e)]. In comparison to a random input field, which has equal contributions from all channels, $w(\tau) = 1/N$, the optimized field for maximum $S$ has greatly enhanced contributions from the high transmission channels and reduced contributions from the low-transmission channels [Fig. 4(a)]. While the maximum transmission channel has the largest weight, a few channels with slightly lower transmission also make significant contributions. Thus, the energy density distribution $I(z)$ is slightly lower than that of the maximum transmission channel, and shifted a bit towards the front end of the waveguide [Fig. 4(b)]. As shown in Fig. 4(a), the weight $w(\tau)$ increases exponentially with $\tau$, in contrast to the linear increase of $w$ with $\tau$ in the case of focusing (maximizing intensity of a single speckle) through a random medium. This difference indicates

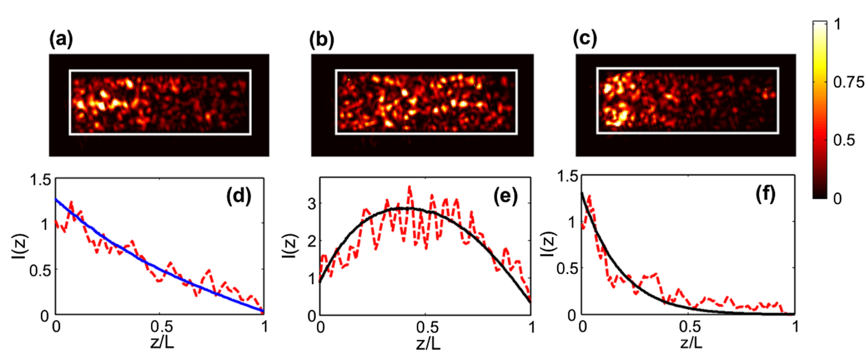


FIG. 3. Experimental control of the intensity distribution inside the disordered waveguide. (a)–(c) Two-dimensional intensity distribution $I(y,z)$ inside the disordered waveguide shown in Fig. 1 for (a) random input fields, (b) optimized input for maximum light penetration (maximizing $S$), and (c) optimized input for minimum light penetration (minimizing $S$). (d)–(f) The cross-section-averaged intensity $I(z)$ obtained from $I(y,z)$ in (a)–(c). The dashed lines are experimental data and the solid lines are simulation results.

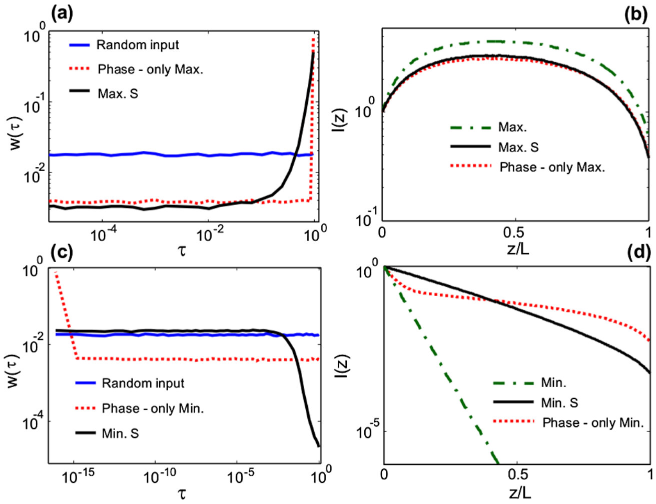


FIG. 4. Numerical simulation of the wave front shaping experiment. (a),(c) Weight $w(\tau)$ of each transmission eigenchannel in the input field obtained by maximizing (a) or minimizing (c) the light penetration into the disordered waveguide with the cost function $S$ (black solid line). For comparison, $w(\tau)$ for the random input field (blue solid line) and for the input field of the maximum (a) or minimum (c) transmission eigenchannel after removal of amplitude modulation (red dotted line) are also shown. (b),(d) Cross-section-averaged intensity distribution $I(z)$ for the maximized (b) or minimized (d) $S$ (black solid line), as well as the maximum (b) or minimum (d) transmission channel with (green dash-dotted line) and without amplitude modulation (red dotted line).

maximizing $S$ is more efficient for enhancing the contribution of the maximum transmission channel over all other channels.

When $S$ is minimized [Figs. 3(c) and 3(f)], the weights of the high-transmission channels are strongly suppressed, especially the highest transmission channel [Fig. 4(c)]. While many low-transmission channels have slightly increased weights as compared to the random input field, none of them becomes dominant. Since the low-transmission channels have exponential decay with different decay lengths, the total intensity distribution $I(z)$ obtained by minimizing $S$ also decays exponentially, but the decay length is longer than that of the minimum transmission channel [Fig. 4(d)].

The numerical simulation confirms that our wave front shaping experiment results in selective coupling of the input light to open or closed channels, which leads to a distinct intensity distribution inside the scattering waveguide. The total transmission is increased from ~4.8% (for random input fields) to ~47% (when $S$ is maximized), and the total energy inside the disordered structure is enhanced 3.7 times. The minimization of $S$ makes the total transmission drop to ~0.1%, and the total energy inside is reduced by a factor of 2.

Finally, we compare numerically the feedback-based approach to the transmission-matrix approach by computing the transmission eigenchannels from the field transmission matrix. With phase-only modulation, the input field for a transmission eigenchannel is decomposed by the waveguide modes, and the amplitudes of the decomposition coefficients are set to a constant. The removal of amplitude modulation mixes the maximum transmission channel with other channels, as seen in Fig. 4(a). While the weight of the maximum transmission channel decreases from unity to $\pi/4$ [32], all other channels have a constant weight $[1-(\pi/4)]/(N-1)$. The cross-section-averaged intensity distribution $I(z)$ is nearly identical to that obtained by maximizing $S$ [Fig. 4(b)]. Similarly, the elimination of amplitude modulation from the minimum transmission channel introduces contributions from all other channels [Fig. 4(c)]. Their weights are equal (independent of their transmission), albeit smaller than that of the minimum transmission channel. Consequently, $I(z)$ displays a rapid decay at shallow depths, due to the dominant contribution from the minimum transmission channel; it is followed by a much slower decay at large depth due to the contributions of the remaining channels including the highly transmitting ones. The total transmission is $\sim 1\%$, approximately an order of magnitude higher than that obtained by minimizing $S$. This is attributed to the stronger suppression of the higher transmission channels by the feedback approach, i.e., the higher the transmission eigenvalue is, the lower the weight. Therefore, with phase-only modulation of the incident wave front, the feedback approach is far more efficient in minimizing the total transmission than the transmission-matrix approach.

In summary, we apply the adaptive wave front shaping technique to on-chip disordered nanostructures. Careful design of the coupling waveguide enables access to all input modes and allows us to reach the maximum or minimum transmission that is achievable with phase-only modulation. Selective excitation of the open or closed channels results in the variation of the optical intensity distribution from an exponential decay to a linear decay and to a profile peaked near the center of the random system. The coherent control of multiple-scattering interference leads to diverse transport behaviors in contrast to universal diffusion, highlighting the possibility of controlling light-matter interactions in turbid media.

We acknowledge Chia-Wei Hsu, Douglas Stone, Hasan Yilmaz, Seng Fatt Liew, and Brandon Redding for useful discussions. This work was supported by the National Science Foundation under Grants No. DMR-1205307 and No. DMR-1205223. Facilities use was supported by YINQE and NSF MRSEC Grant No. DMR-1119826.

[*]yamilov@mst.edu
[†]hui.cao@yale.edu

[1] M. C. W. van Rossum and T. M. Nieuwenhuizen, Rev. Mod. Phys. 71, 313 (1999).

[2] E. Akkermans and G. Montambaux, *Mesoscopic Physics of Electrons and Photons* (Cambridge University Press, Cambridge, England, 2007).
[3] O. N. Dorokhov, Solid State Commun. **51**, 381 (1984).
[4] Y. Imry, Europhys. Lett. **1**, 249 (1986).
[5] M. Davy, Z. Shi, J. Park, C. Tian, and A. Z. Genack, Nat. Commun. **6**, 6893 (2015).
[6] R. Sarma, A. Yamilov, S. F. Liew, M. Guy, and H. Cao, Phys. Rev. B **92**, 214206 (2015).
[7] K. Vynck, M. Burresi, F. Riboli, and D. S. Wiersma, Nat. Mater. **11**, 1017 (2012).
[8] D. S. Wiersma, Nat. Photonics **7**, 188 (2013).
[9] V. Y. F. Leung, A. Lagendijk, T. W. Tukker, A. P. Mosk, W. L. Ijzerman, and W. L. Vos, Opt. Express **22**, 8190 (2014).
[10] X. Cheng and A. Z. Genack, Opt. Lett. **39**, 6324 (2014).
[11] Q. Song, S. Xiao, Z. Xu, V. M. Shalaev, and Y. L. Kim, Opt. Lett. **35**, 2624 (2010).
[12] J. Yoon, M. Lee, K. Lee, N. Kim, J. M. Kim, J. Park, H. Yu, C. Choi, W. Do Heo, and Y. Park, Sci. Rep. **5**, 13289 (2015).
[13] I. M. Vellekoop and A. P. Mosk, Phys. Rev. Lett. **101**, 120601 (2008).
[14] A. P. Mosk, A. Lagendijk, G. Lerosey, and M. Fink, Nat. Photonics **6**, 283 (2012).
[15] W. Choi, A. P. Mosk, Q. Han Park, and W. Choi, Phys. Rev. B **83**, 134207 (2011).
[16] A. Peña, A. Girschik, F. Libisch, S. Rotter, and A. A. Chabanov, Nat. Commun. **5**, 3488 (2014).
[17] S. F. Liew, S. M. Popoff, A. P. Mosk, W. L. Vos, and H. Cao, Phys. Rev. B **89**, 224202 (2014).
[18] S. M. Popoff, G. Lerosey, R. Carminati, M. Fink, A. C. Boccara, and S. Gigan, Phys. Rev. Lett. **104**, 100601 (2010).
[19] Z. Shi and A. Z. Genack, Phys. Rev. Lett. **108**, 043901 (2012).
[20] M. Kim, Y. Choi, C. Yoon, W. Choi, J. Kim, Q. H. Park, and W. Choi, Nat. Photonics **6**, 581 (2012).
[21] H. Yu, T. R. Hillman, W. Choi, J. O. Lee, M. S. Feld, R. R. Dasari, and Y. K. Park, Phys. Rev. Lett. **111**, 153902 (2013).
[22] B. Gerardin, J. Laurent, A. Derode, C. Prada, and A. Aubry, Phys. Rev. Lett. **113**, 173901 (2014).
[23] A. Goetschy and A. D. Stone, Phys. Rev. Lett. **111**, 063901 (2013).
[24] S. M. Popoff, A. Goetschy, S. F. Liew, A. D. Stone, and H. Cao, Phys. Rev. Lett. **112**, 133903 (2014).
[25] O. S. Ojambati, H. Yilmaz, A. Lagendijk, A. P. Mosk, and W. L. Vos, New J. Phys. **18**, 043032 (2016).
[26] R. Sarma, A. Yamilov, P. Neupane, and H. Cao, Phys. Rev. B **92**, 180203 (2015).
[27] See Supplemental Material at http://link.aps.org/supplemental/10.1103/PhysRevLett.117.086803 for detail description about the experimental setup, structure design and numerical simulations.
[28] M. Kim, W. Choi, Y. Choi, C. Yoon, and W. Choi, Opt. Express **23**, 12648 (2015).
[29] H. Yu, J. Park, K. Lee, J. Yoon, K. Kim, S. Lee, and Y. Park, Curr. Appl. Phys. **15**, 632 (2015).
[30] I. M. Vellekoop, Opt. Express **23**, 12189 (2015).
[31] C. W. Groth, M. Wimmer, A. R. Akhmerov, and X. Waintal, New J. Phys. **16**, 063065 (2014).
[32] I. M. Vellekoop, E. G. Van Putten, A. Lagendijk, and A. P. Mosk, Opt. Express **16**, 67 (2008).